

PCCP

Accepted Manuscript



This is an *Accepted Manuscript*, which has been through the Royal Society of Chemistry peer review process and has been accepted for publication.

Accepted Manuscripts are published online shortly after acceptance, before technical editing, formatting and proof reading. Using this free service, authors can make their results available to the community, in citable form, before we publish the edited article. We will replace this *Accepted Manuscript* with the edited and formatted *Advance Article* as soon as it is available.

You can find more information about *Accepted Manuscripts* in the [Information for Authors](#).

Please note that technical editing may introduce minor changes to the text and/or graphics, which may alter content. The journal's standard [Terms & Conditions](#) and the [Ethical guidelines](#) still apply. In no event shall the Royal Society of Chemistry be held responsible for any errors or omissions in this *Accepted Manuscript* or any consequences arising from the use of any information it contains.

Anisotropic charge-transfer effect in the asymmetric Fe(CN)₅NO octahedron of sodium nitroprusside: a soft x-ray absorption spectroscopy study[†]

Yūsuke Nanba,^a Daisuke Asakura,^{*a} Masashi Okubo,^a Haoshen Zhou,^a Kenta Amemiya,^b Kozo Okada,^c Per-Anders Glans,^d Catherine A. Jenkins,^d Elke Arenholz,^d and Jinghua Guo^d

Received Xth XXXXXXXXXXXX 20XX, Accepted Xth XXXXXXXXXXXX 20XX

First published on the web Xth XXXXXXXXXXXX 200X

DOI: 10.1039/b000000x

Electronic structure of Na₂[Fe(CN)₅NO]·2H₂O (Sodium nitroprusside: SNP) was investigated by using soft x-ray absorption (XA) spectroscopy. The Fe *L*_{2,3}-edge XA spectrum for SNP exhibited distinct and very large satellite peaks each for *L*₃ and *L*₂ region, which is different from the spectra for hexacyanoferrates and the other iron compounds. A configuration-interaction full-multiplet calculation, in which the ligand molecular orbitals for the C_{4v} symmetry were taken into account, revealed the Fe²⁺ low-spin state with very strong metal-to-ligand charge-transfer effect from the Fe 3*d* to NO 2*p* orbitals.

1 Introduction

Nitroprusside (NP) compounds such as Na₂[Fe(CN)₅NO]·2H₂O (Sodium NP: SNP) and *M*[Fe(CN)₅NO]·*n*H₂O (*M*: 3*d* transition metal) have been extensively studied in various fields such as photochemistry and holography^{1,2}. For example, SNP exhibits photo-induced reduction/oxidation reactions on the NO⁺ ligand by ultraviolet (UV) or visible light irradiation: NO⁺ ⇌ NO ⇌ NO⁻^{3,4}. The photo-induced phase transitions should originate from interactions between NO and Fe in the asymmetric Fe(CN)₅NO octahedron^{5–7}. The coordination environment and the electronic structure of the Fe atom in NP compounds should be quite unique due to the asymmetry.

The Fe 3*d* electronic structures of NP compounds have been investigated by various methods: theoretical calculations^{8–11}, infrared spectroscopy^{12–15}, optical absorption in visible-UV region^{15–17}, Mössbauer spectroscopy^{13,18} and hard x-ray absorption spectroscopy at the Fe *K* edge⁵. However, those experimental techniques are insufficient to directly observe the Fe 3*d* orbital, resulting in that the theoretical predictions have not been evaluated precisely. On the other hand, soft x-ray ab-

sorption (XA) spectroscopy at the transition-metal (TM) *L*_{2,3} edges (2*p* → 3*d* absorption) can provide direct information on the TM 3*d* orbitals. The electronic-structure parameters including the crystal-field splitting and the charge-transfer (CT) energy can be obtained by analyzing the *L*_{2,3}-edge XA spectra by using multiplet calculations.

Fe *L*_{2,3}-edge XA spectroscopy studies to reveal the Fe 3*d* electronic structure and the CT between the Fe 3*d* and ligand 2*p* orbitals for SNP have not been reported yet. The valence of the NO group was theoretically predicted to be rather +0.6 than +1.0⁹, implying an anisotropic CT effect in the Fe(CN)₅NO octahedron, i.e., a strong metal-to-ligand CT (MLCT) from the Fe to the NO group. To clarify the Fe 3*d* electronic structure and the CT effects in SNP, Fe *L*_{2,3}-edge XA spectroscopy and detailed analyses by multiplet calculation are essential. In studying the electronic structure of SNP, analogies to hexacyanoferrates which have a symmetric Fe(CN)₆ octahedron in the unit cell should provide us fruitful information.

The XA spectroscopy measurements were performed for the hexacyanoferrates: K₃[Fe(CN)₆] and K₄[Fe(CN)₆] which are typical cyano complexes¹⁹. The Fe *L*_{2,3}-edge XA spectra of K₄[Fe(CN)₆] and K₃[Fe(CN)₆] were reproduced by CT multiplet calculation¹⁹. The analyses by the multiplet calculations have revealed strong MLCT effects in addition to ligand-to-metal CT (LMCT) effects for the hexacyanoferrates. In order to further understand the electronic structure and the CT effects in the hexacyanoferrates and the related cyano complexes, we have developed configuration-interaction full-multiplet (CIFM) calculation in which the ligand molecular orbitals are taken into account^{20–22}.

^a Energy Technology Research Institute, National Institute of Advanced Industrial Science and Technology, Tsukuba, Ibaraki 305-8568, Japan.

E-mail: daisuke-asakura@aist.go.jp

^b Photon Factory, IMSS, High Energy Accelerator Research Organization, Tsukuba, Ibaraki 305-0801, Japan.

^c The Graduate School of Natural Science and Technology, Okayama University, Okayama 700-8530, Japan.

^d Advanced Light Source, Lawrence Berkeley National Laboratory, Berkeley, California 94720, USA.

[†] Electronic Supplementary Information (ESI) available: A detailed description of making a molecular orbital. See DOI: 10.1039/b000000x/

In this paper, we report the Fe $L_{2,3}$ -edge XA spectroscopy study for SNP. The XA spectra were analyzed by using the CIFM calculations for the C_{4v} symmetry. Moreover, the calculated electronic-structure parameters for SNP are compared with those for hexacyanoferrates: $K_3[Fe(CN)_6]$ with the Fe^{3+} low-spin (LS) state and $K_4[Fe(CN)_6]$ with the Fe^{2+} LS state.

2 Experimental method

The SNP sample purchased from Wako Pure Chemical Industries, Ltd. was powdered and fixed on a sample holder by carbon tape. The XA spectroscopy measurement was performed at bending magnet beamlines, BL-7A of the Photon Factory and BL 6.3.1 of the Advanced Light Source. The total energy resolution was $E/\Delta E \sim 1500$. To suppress the radiation damage for the sample, we set the slit width of the spectrometer as narrow as the signal-to-noise ratio was not deteriorated. We also confirmed that the spectral shape was not dependent on sample positions. Moreover, several XAS scans were performed on one sample position, and no difference in the XA spectral shape was found between the first and last scans. Thus, the radiation damage problem is not an issue in this study. All the measurements were carried out at room temperature.

3 Theoretical model

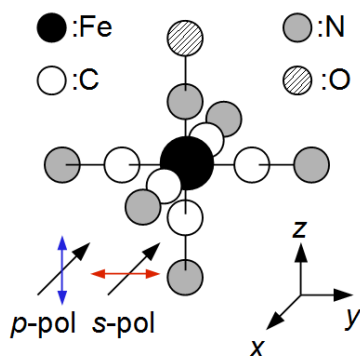


Fig. 1 Octahedral $[Fe(CN)_5NO]^{2-}$ cluster. The NO group is located along z -axis in the present definition. The x -ray electric field polarizations (p -pol and s -pol) are also depicted for an incident x -ray along x -axis. In the Fe L -edge XA spectroscopy measurement, the domains in the powdered sample are randomly oriented to the incoming beam.

The CIFM calculation for the Fe $3d$ electronic structure of SNP was carried out by using the cluster model in Fig. 1. NO is located along the z -axis. Hereafter, the N atom in the NO

ligand is expressed as N' . The Hamiltonian is given by

$$\mathcal{H} = \mathcal{H}_0 + \mathcal{H}_1 + \mathcal{H}_2, \quad (1)$$

where

$$\begin{aligned} \mathcal{H}_0 = & \sum_{\gamma,\sigma} [\varepsilon_d(\gamma) - Q \sum_{m,\sigma'} (1 - n_{p,m\sigma'})] n_{d,\gamma\sigma} \\ & + \sum_{m,\sigma} \varepsilon_p n_{p,m\sigma} + U \sum_{\gamma} n_{d,\gamma\uparrow} n_{d,\gamma\downarrow} \\ & + \sum_{\gamma>\gamma',\sigma,\sigma'} (U' - J\delta_{\sigma\sigma'}) n_{d,\gamma\sigma} n_{d,\gamma'\sigma'} \end{aligned} \quad (2)$$

and

$$\mathcal{H}_1 = \sum_{j,\gamma,\sigma} \varepsilon_p(j\gamma) n_{p,j\gamma\sigma} + \sum_{j,\gamma,\sigma} V_{pd}(j\gamma) (d_{\gamma\sigma}^\dagger P_{j\gamma\sigma} + h.c.). \quad (3)$$

The symmetry γ indicates a_1 , b_1 , b_2 or e irreducible representations in C_{4v} . The first term in Eq. (2) represents the Fe $3d$ state with $\varepsilon_d(\gamma)$ being the one-electron energy level and Q being the Coulomb attraction caused by the Fe $2p$ core hole. The second term denotes the Fe $2p$ states. The third and last terms describe the Coulomb interaction with U and the exchange interaction with J between the Fe $3d$ electrons.

\mathcal{H}_1 in Eq. (1) includes the molecular orbitals (MOs) consisting of C, N, and O $2p$ orbitals and the hybridization between the Fe $3d$ and the MOs. $P_{j\gamma\sigma}^\dagger$ and $n_{p,j\gamma\sigma}$ in Eq. (3) represent the creation and number operators for the j th MO with orbital symmetry γ and spin σ . We used the transfer integrals for C-C, C-N, N'-C, and N'-O ($(pp\sigma)_{CC}$, $(pp\sigma)_{CN}$, $(pp\sigma)_{NC}$, and $(pp\sigma)_{NO}$) to obtain the MO energy ε_p . The hybridization strengths between the Fe $3d$ and the MOs could be derived from combining the MO wave functions with the transfer integrals for Fe-C and Fe-N ($(pd\sigma)_C$ and $(pd\sigma)_N$). The details are described in the Supporting Information and the previous studies^{20,21}.

\mathcal{H}_2 in Eq. (1) includes the multipole part of the Fe $3d$ -Fe $3d$ and Fe $3d$ -Fe $2p$ Coulomb interactions that are not described in Eq. (2) and the spin-orbit interactions for the Fe $3d$ and Fe $2p$ orbitals. We evaluate the Slater integrals by using Cowan's code²³ and reduce them to 85% in order to take account of the effect of the configuration interactions not included in the present study.

The bases to diagonalize the Hamiltonian in the ground state consist of $d^6 [(t_{2g})^6: Fe^{2+} \text{ LS configuration}]$, $d^5\bar{L}$, $d^7\bar{L}$, $d^4\bar{L}^2$, $d^6\bar{L}\bar{L}$, and $d^8\bar{L}^2$ electron configurations. Note that \bar{L} and \bar{L}^2 denote the ligand electron and hole, respectively. The XA spectrum was calculated using the Fermi's golden rule²⁴ expressed as

$$I(E) = \sum_i |\langle f_i | T | g \rangle|^2 \delta(E - E_{f_i} + E_g) \quad (4)$$

where $|g\rangle$ and $|f\rangle$ are the ground (initial) and final states of the XA spectrum, and E_g and E_f are the corresponding energies. T denotes the electric dipole operator, which leads the

polarization-dependent XA spectra^{21,25,26}. In our calculation, the *p*-polarization (*p*-pol) and *s*-polarization (*s*-pol) were defined as being parallel and perpendicular to the *z*-axis as displayed in Fig. 1. We averaged these polarizations as $\{(p\text{-pol})+2(s\text{-pol})\}/3$ for a comparison with the experimental result, since the domains in the powdered sample are randomly oriented to the incoming beam. The weight of the *s*-pol was doubled because the orthogonal two axes should be taken into account for the in-plane geometry. The detail of the corresponding electric dipole transition operators was described in the previous study²¹.

The wave function was numerically calculated by the Lanczos method²⁷. The theoretical line spectra thus obtained were convoluted, using the Lorentzian and Gauss functions (with each width of 0.4 eV).

4 Results

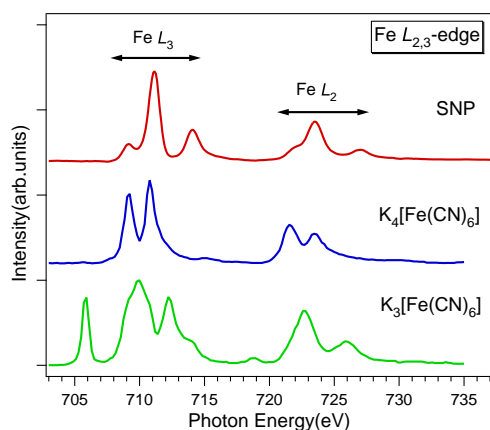


Fig. 2 Experimental Fe $L_{2,3}$ -edge XA spectrum of SNP. The spectra for $K_4[Fe(CN)_6]$ and $K_3[Fe(CN)_6]$ by Hocking et al.¹⁹ are also displayed.

Figure 2 shows the Fe $L_{2,3}$ -edge XA spectrum of SNP together with those of $K_4[Fe^{2+}(CN)_6]$ and $K_3[Fe^{3+}(CN)_6]$ ¹⁹. The spectrum for SNP has an intense main peak at 711 eV with two satellite peaks at 709 and 714 eV for the L_3 edge. Similar peaks were observed for the L_2 edge. This spectrum is totally different from the Fe $L_{2,3}$ -edge XA spectra for iron oxides^{28,29} and most Fe compounds^{30–34}. In $K_3[Fe(CN)_6]$, a large peak attributed to partially-unoccupied t_{2g} orbital appears at 706 eV, which is completely different from SNP and $K_4[Fe(CN)_6]$. In $K_4[Fe(CN)_6]$, the MLCT gives a great influence on the Fe $3d$ electronic structure, which forms the large satellite peak at 711 eV. The spectrum of SNP also has the large satellite peaks at 714 and 727 eV, which suggests the strong MLCT effect as in $K_4[Fe(CN)_6]$. However, the peak positions and the intensities in SNP largely differ from those

in $K_4[Fe(CN)_6]$ with O_h symmetry. In SNP, the lower symmetry of the $[Fe(CN)_5NO]$ octahedron should cause anisotropic CT effects.

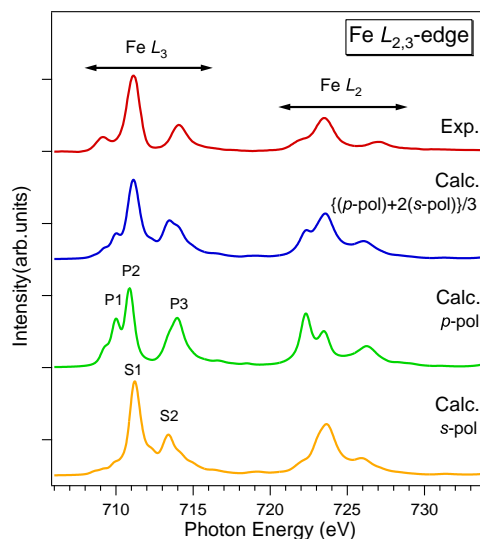


Fig. 3 Theoretical spectra of the $[Fe(CN)_5NO]^{2-}$ cluster for *p*-pol and *s*-pol, and an averaged spectrum. Experimental Fe $L_{2,3}$ -edge XA spectrum of SNP is also shown.

The CIFM calculation for the $[Fe(CN)_5NO]^{2-}$ -cluster model with C_{4v} symmetry was carried out to analyze the Fe $L_{2,3}$ -edge XA spectrum. The best fitted polarization-dependent spectra and the spectrum averaged for the *p*-pol and *s*-pol are shown in Fig. 3. The averaged spectrum reproduces the characteristics in the experimental result well. The spectrum for the *p*-pol has a peak at the low-energy side for both the L_3 and L_2 edges. In the calculation, the spectrum for the *p*-pol reflects the unoccupied $3d$ orbitals which extend along the *z*-axis²¹. Accordingly, the XA spectrum for the *p*-pol gives direct information on the $3d(yz)$, $3d(zx)$, and $3d(3z^2 - r^2)$ orbitals, which hybridize with the NO ligand. Since the local symmetry is C_{4v} , the degeneracy of the MO energy levels is lifted, compared with the O_h case. This is reflected in the number of satellite peaks. On the other hand, the spectrum for the *s*-pol shows no peak at the energy region lower than the most intense peak. The spectrum for the *s*-pol reflects the unoccupied $3d$ orbitals which extend in the *xy*-plane. The corresponding orbitals are the $3d(xy)$ and $3d(x^2 - y^2)$ ones that are only hybridized with the ligands which is symmetric with respect to the *xy*-plane. Thus, the number of peaks for the *s*-pol spectrum is the same as that in $K_4[Fe(CN)_6]$ with the O_h symmetry. Hereafter, in the spectrum for the *p*-pol, the main peak at 711 eV is denoted as P2 and the satellite peaks at 709 and 714 eV are denoted as P1 and P3 (Fig. 3). In the spectrum for the *s*-pol, the main peak at 711.5 eV and satellite peak at 713.5 eV are denoted as S1 and S2, respectively.

Table 1 Electronic-structure parameters of $[\text{Fe}(\text{CN})_5\text{NO}]^{2-}$, $[\text{Fe}(\text{CN})_6]^{4-}$, and $[\text{Fe}(\text{CN})_6]^{3-}$ clusters (in eV). $(pd\pi)$ and $(pp\pi)$ can be calculated according to the relations of $(pd\pi)/(pd\sigma) = -1.0/2.2$ and $(pp\pi)/(pp\sigma) = -1.0/4.0^{35}$, respectively.

	$[\text{Fe}(\text{CN})_5\text{NO}]^{2-}$	$[\text{Fe}(\text{CN})_6]^{4-}$	$[\text{Fe}(\text{CN})_6]^{3-}$
Δ	3.0	2.7	1.4
U	6.7	6.7	6.9
J	0.77	0.77	0.86
Q	4.0	4.0	4.0
$10Dq$	3.3	3.9	4.0
$(pd\sigma)_C$	-2.4	-2.4	-2.5
$(pd\sigma)_N$	-3.6	-	-
$(pp\sigma)_{CC}$	1.0	1.0	1.0
$(pp\sigma)_{CN}$	8.0	8.0	8.0
$(pp\sigma)_{NC}$	1.5	-	-
$(pp\sigma)_{NO}$	3.5	-	-
ϵ_C	0.0	0.0	0.0
ϵ_N	-2.5	-2.5	-2.5
ϵ_O	-4.0	-	-

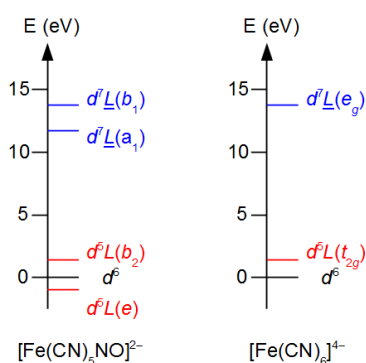


Fig. 4 Relative energy levels for LMCT (blue) and MLCT (red) electron configurations in $[\text{Fe}(\text{CN})_5\text{NO}]^{2-}$ and $[\text{Fe}(\text{CN})_6]^{4-}$ clusters. The configurations, which show the lowest CT energy in the symmetry, are depicted.

Table 1 shows the electronic-structure parameters of the $[\text{Fe}(\text{CN})_5\text{NO}]^{2-}$ cluster used in the CIFM calculation, which includes the CT energy Δ , the Coulomb interaction U , the exchange interaction J , the core-hole potential Q , and the crystal field splitting $10Dq$. The definition of Δ is described in Ref. 21, where the O_h symmetry was assumed. The parameter values to reproduce the Fe $L_{2,3}$ -edge XA spectrum of $\text{K}_4[\text{Fe}(\text{CN})_6]$ and $\text{K}_3[\text{Fe}(\text{CN})_6]$ in Fig. 2 are also shown in Table 1²⁰. $10Dq$ of 3.3 eV is large enough to stabilize the Fe^{2+} LS state in $[\text{Fe}(\text{CN})_5\text{NO}]^{2-}$, but is slightly smaller than those of $[\text{Fe}^{2+}(\text{CN})_6]^{4-}$ and $[\text{Fe}^{3+}(\text{CN})_6]^{3-}$ clusters. The absolute value of transfer integral for Fe-N', $(pd\sigma)_N$ ($= -3.6$ eV), is larger than that for Fe-C, $(pd\sigma)_C$ ($= -2.4$ eV), and is close to the value in the cluster model analysis of the Fe L -edge resonant x-ray emission spectra of cyanomet myoglobin (-3.18

eV)³⁶. The transfer integral for N'-O, $(pp\sigma)_{NO}$ ($= 3.5$ eV), is less than half that for C-N, $(pp\sigma)_{CN}$ ($= 8.0$ eV), which results in that the energy separation between the bonding- and antibonding-type MOs becomes small compared with that of $\text{K}_4[\text{Fe}(\text{CN})_6]$. The CT from the MO to the Fe $3d(3z^2 - r^2)$ has the lowest LMCT energy $\Delta(a_1)$ (corresponding to the energy difference between the $d^7\bar{L}(a_1)$ and d^6 levels as shown in Fig. 4) expressed as

$$\Delta(a_1) = \Delta + 6Dq - \epsilon_P(a_1) + \epsilon_C. \quad (5)$$

The CT from the Fe $3d(yz)$ [$3d(zx)$] to the MO has lowest the MLCT energy $\Delta^*(e)$ (corresponding to the energy difference between the $d^5\bar{L}(e)$ and d^6 levels as shown in Fig. 4) expressed as

$$\Delta^*(e) = U - 5J - \Delta(a_1) + 10Dq + \epsilon_P(e) - \epsilon_P(a_1). \quad (6)$$

The derivation of $\Delta^*(e)$ and $\Delta(a_1)$ is described in Ref. 21. $\Delta^*(e)$ calculated to be -1.0 eV from Eq. (6) is much smaller than $\Delta(a_1)$ calculated to be 11.7 eV from Eq. (5), which indicates that the $d^5\bar{L}$ is the dominant electron configuration. The negative $\Delta^*(e)$ indicates that the energy level of the $d^5\bar{L}$ electron configuration is lower than that of the d^6 one, while the d^6 electron configuration is energetically the lowest in $[\text{Fe}(\text{CN})_6]^{4-}$ cluster (Fig. 4). The MLCT effect should be very strong in $[\text{Fe}(\text{CN})_5\text{NO}]^{2-}$ cluster.

Table 2 Weights of each configuration in the ground state (in percent), average $3d$ electron number $\langle n_d \rangle$, and calculated valences of the CN and NO ligands in $[\text{Fe}(\text{CN})_5\text{NO}]^{2-}$, $[\text{Fe}(\text{CN})_6]^{4-}$, and $[\text{Fe}(\text{CN})_6]^{3-}$ clusters.

	$[\text{Fe}(\text{CN})_5\text{NO}]^{2-}$	$[\text{Fe}(\text{CN})_6]^{4-}$	$[\text{Fe}(\text{CN})_6]^{3-}$
d^6	28.7	43.5	d^5 53.9
$d^7\bar{L}$	4.3	5.1	$d^6\bar{L}$ 16.9
$d^5\bar{L}$	49.4	40.3	$d^4\bar{L}$ 19.3
$d^8\bar{L}^2$	0.1	0.1	$d^7\bar{L}^2$ 0.9
$d^6\bar{L}\bar{L}$	9.4	6.1	$d^5\bar{L}\bar{L}$ 8.0
$d^4\bar{L}^2$	8.0	4.9	$d^3\bar{L}^2$ 1.0
$\langle n_d \rangle$	5.39	5.55	$\langle n_d \rangle$ 4.97
CN_{xy}	-0.982	-1.075	CN_{xy} -1.005
CN_z	-1.034	-1.075	CN_z -1.005
NO	0.352	-	NO -

Table 2 shows the relative weights of each electron configuration in the ground state obtained from the CIFM calculation, together with the cases of hexacyanoferrates. The weight of the $d^5\bar{L}$ is considerably large (49.4 %) in SNP due to the negative MLCT energy, and the total weight of the d^6 and $d^5\bar{L}$ is up to 78.1 % in the ground-state wave function, which indicates that the Fe $L_{2,3}$ -edge XA spectrum is subject to these electron configurations. Thus, the average Fe $3d$ electron number, $\langle n_d \rangle$, is close to five rather than six.

Table 2 also shows the calculated valences of the NO ligand and the CN ligands in the xy -plane and along the z -axis. Hereafter, the CN ligands in the xy -plane and along the z -axis are denoted as CN_{xy} and CN_z ligands, respectively. In $[Fe(CN)_6]^{4-}$ for $K_4[Fe(CN)_6]$, the valences of the CN ligands are isotropic and the value of -1.075 suggests the strong MLCT effect. The valence of the CN_z ligand in the $[Fe(CN)_5NO]^{2-}$ cluster is close to that in $[Fe(CN)_6]^{4-}$. On the other hand, the valence of the CN_{xy} ligand is -0.982 , while that for $[Fe(CN)_6]^{4-}$ was -1.075 . Thus, the MLCT from the Fe $3d$ to the CN_{xy} is weak compared with that in $[Fe(CN)_6]^{4-}$. The valence of the NO ligand was calculated to be $+0.352$, which largely deviated from the nominal valence of $+1.0$ for NO, indicating very strong MLCT. A similar result has been reported by Trautwein *et al.*: the valence of the NO ligand in SNP was determined to be $+0.613$ in their semiempirical self-consistent-field MO calculations⁹. The deviation from the nominal valence of NO, $\delta n_{NO} = 0.648$, nearly corresponds to the deviation of the calculated $\langle n_d \rangle$ from the nominal valence of Fe^{2+} : $\delta n_{Fe} = 6 - \langle n_d \rangle = 0.61$. This result again indicates that the MLCT from NO to Fe is much dominant than the MLCT from Fe to CN and that the strength of the MLCT between Fe and CN is comparable to that of the LMCT. The MLCT effect for SNP is stronger than that for $K_4[Fe(CN)_6]$, since δn_{Fe} for SNP is larger than δn_{Fe} for $[Fe(CN)_6]^{4-}$.

To attribute the peaks of the calculated spectrum to the electron configurations, we investigated the Δ dependence of the Fe $L_{2,3}$ -edge XA spectrum for the $[Fe(CN)_5NO]^{2-}$ cluster [Figs. 5(a) and 5(b)] and the Δ dependences of the d^6 and d^5L weights in the ground state [Fig. 5(c)], where the other parameters are fixed to the values listed in Table 1. Clarifying the weights in the ground state for each Δ help us to discuss the Δ dependence of XA spectrum, because the XA intensities strongly depends on the ground-state wave function²⁰. The relative weights of each electron configuration in the ground state as shown in Table 2 indicates that the Fe $L_{2,3}$ -edge XA spectrum is subject to the d^6 and d^5L electron configurations. Thus, the characteristic peaks of the calculated spectrum can be attributed to the final state for these electron configurations. The corresponding final states of XA spectrum for the two electron configurations are $\underline{c}d^7$ and $\underline{c}d^6L$. Note that \underline{c} denotes a core hole on Fe $2p$ orbital.

Figure 5(a) shows the Δ dependence of the Fe $L_{2,3}$ -edge XA spectrum for the p -pol; the spectrum for $\Delta = 3.0$ eV is the same as that shown in Fig. 3. Peak P1 becomes small as Δ increases whereas peaks P2 and P3 become large. As Δ increases from -1.0 to 5.0 eV, the weight of the d^6 in the ground state decreases from 48% to 18%, while that of the d^5L increases from 26% to 57% [Fig. 5(c)]. The relationship between the Δ dependence of the spectra and that of the weights in the ground state indicates that peak P1 reflects the $\underline{c}d^7$ electron configuration in the final state of XA spectrum and peaks P2 and P3

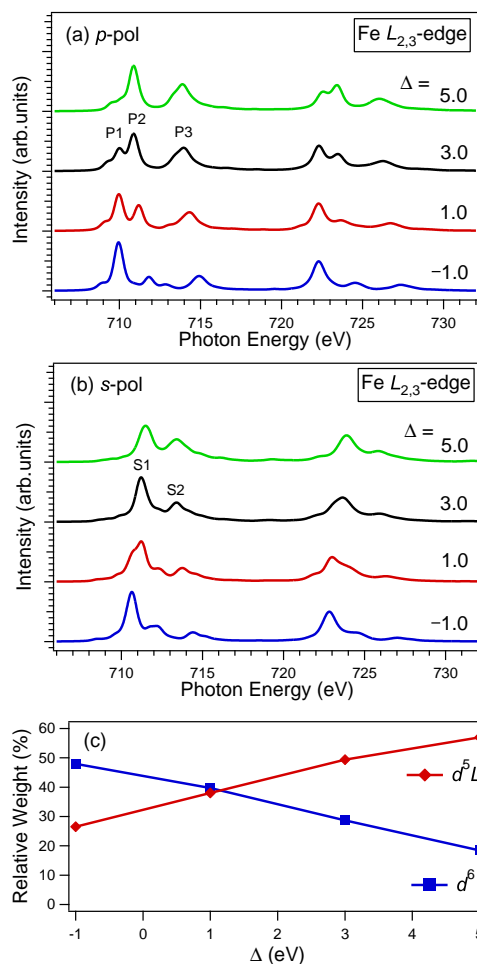


Fig. 5 Δ dependences of Fe $L_{2,3}$ -edge XA spectra calculated for (a) p - and (b) s -pol geometries. The case of $\Delta = 3.0$ eV is the same as FIG. 3. The relative weights of d^6 and d^5L configurations in the ground state for the corresponding Δ values are shown in (c).

originate from the \underline{cd}^6L electron configuration. The energy separation between P1 and P2 becomes small as Δ increases because the energy difference from the \underline{cd}^7 to the \underline{cd}^6L is proportional to $-\Delta$. The energy separation between peaks P2 and P3 is proportional to the energy difference of the MOs. The lowest energy level in the unoccupied molecular orbitals that hybridize with the Fe $3d(yz)$ and/or $3d(zx)$, i.e. the energy level of the $d^5L(e)$ shown in Fig. 4, changes largely, depending on the $(pp\sigma)_{\text{NO}}$ value, while the others are dependent on the $(pp\sigma)_{\text{CN}}$ one. The lowest energy level corresponds with the NO ligand and the others are assigned to the CN ligand. Thus, peaks P2 and P3 reflect the MLCT effects of the NO and CN_z ligands, respectively.

As Figure 5(b) indicates, peaks S1 and S2 for the s -pol have the similar Δ dependence to peaks P1 and P2, respectively. The energy separation between S1 and S2 also has the same dependence as that between P1 and P2. Thus, peak S1 is attributed to the \underline{cd}^7 electron configuration, while peak S2 is caused by the \underline{cd}^6L one. In addition, a small peak appears at 712 eV between peaks S1 and S2 in the cases of $\Delta = 1.0$ and -1.0 eV. This peak appears because of the multiplet splitting effects. Peak S2 should be ascribed to the MLCT effects of the CN_{xy} ligands. Although the CN_{xy} ligand in the case of $\Delta = 3.0$ eV has the LMCT character in total (the valence of -0.982 as shown in Table 2), the MLCT channel should also exist. Note that the MLCT effect can predominantly be detected in XA spectrum compared to the LMCT one, since XA spectrum observes the unoccupied state through the absorption process. For $\Delta = 3.0$ eV, the energy positions of peaks P1 and S1 are different although both the two peaks reflect the \underline{cd}^7 electron configuration. This is due to the large anisotropic hybridization.

5 Conclusions

The Fe $L_{2,3}$ -edge XA spectroscopy study with the CIFM calculation was performed to reveal the Fe $3d$ electronic structure of SNP. The Fe $L_{2,3}$ -edge XA spectrum of SNP was attributed to the Fe^{2+} LS state with the strong CT effects. The CIFM calculation for the $[\text{Fe}(\text{CN})_5\text{NO}]^{2-}$ cluster model revealed the asymmetric CTs due to the existence of the NO group in SNP. The hybridization between the Fe and the NO ligand is much stronger than that between the Fe and the CN one in SNP. The average Fe $3d$ electron number (n_d) was calculated to be 5.39 in agreement with the strong MLCT effect to NO. Each peak in the XA spectrum can be understood as being the \underline{cd}^7 and \underline{cd}^6L final states. The present study demonstrates that a combined use of XA spectroscopy and CIFM calculation has a high potential to clarify the anisotropic electronic structure of TM complexes with low symmetries.

Acknowledgements

This work was done under the approvals of the Photon Factory Program Advisory Committee (Proposal Nos. 2010G038 and 2012G107) and of the Advanced Light Source (Proposal No. 04907R). This work was also conducted based on the Japan-U.S. cooperation project for research and standardization of Clean Energy Technologies. The Advanced Light Source is supported by the Director, Office of Science, Office of Basic Energy Science, of the U.S. Department of Energy under Contract No. DE-AC02-05CH11231.

References

- 1 M. Imlau, R. Schieder, R. A. Rupp and T. Woike, *Appl. Phys. Lett.*, 1999, **75**, 16–18.
- 2 M. Imlau, T. Woike, R. Schieder and R. A. Rupp, *Euro. Phys. Lett.*, 2001, **53**, 471–477.
- 3 P. Coppens, I. Novozhilova and A. Kovalevsky, *Chem. Rev.*, 2002, **102**, 861–883.
- 4 A. C. Montenegro, V. T. Amorebieta, L. D. Slep, D. F. Martín, F. Roncaroli, D. H. Murgida, S. E. Bari and J. A. Olabe, *Angew. Chem. Int. Ed.*, 2009, **48**, 4213–4216.
- 5 W. Gädeke, E. E. Koch, G. Dräger, R. Frahm and V. Saile, *Chem. Phys.*, 1988, **124**, 113–119.
- 6 M. R. Pressprich, M. A. White, Y. Vekhter and P. Coppens, *J. Am. Chem. Soc.*, 1994, **116**, 5233–5238.
- 7 T. Matsuda, J. Kim and Y. Moritomo, *RSC Adv.*, 2011, **1**, 1716–1720.
- 8 P. T. Manoharan and H. B. Gray, *J. Am. Chem. Soc.*, 1965, **87**, 3340–3348.
- 9 A. Trautwein, F. E. Harris and I. Dézsi, *Theoret. Chim. Acta.*, 1974, **35**, 231–236.
- 10 B. Delley, J. Schefer and T. Woike, *J. Chem. Phys.*, 1997, **107**, 10067–10074.
- 11 P. Boulet, M. Buchs, H. Chermette, C. Daul, F. Gilardoni, F. Rogemond, C. W. Schlöpfer and J. Weber, *J. Phys. Chem. A*, 2001, **105**, 8991–8998.
- 12 J. A. Guida, O. E. Piro and P. J. Aymonino, *Solid State Commun.*, 1986, **57**, 175–178.
- 13 P. Gütllich, Y. Garcia and T. Woike, *Coord. Chem. Rev.*, 2001, **219–221**, 839–879.
- 14 M. E. C. Villalba, J. A. Güida, E. L. Varetti and P. J. Aymonino, *Inorg. Chem.*, 2003, **42**, 2622–2627.
- 15 Z. Tahri, R. Lepski, K.-Y. Hsieh, E.-E. Bendeif, S. Pillet, P. Durand, T. Woike and D. Schaniel, *Phys. Chem. Chem. Phys.*, 2012, **14**, 3775–3781.
- 16 T. Woike, W. Krasser, P. S. Bechthold and S. Haussühl, *Solid State Commun.*, 1983, **45**, 499–502.
- 17 T. Woike, W. Krasser, P. S. Bechthold and S. Haussühl, *Solid State Commun.*, 1983, **45**, 503–506.
- 18 T. Woike, M. Imlau, V. Angelov, J. Schefer and B. Delley, *Phys. Rev. B*, 2000, **61**, 12249–12260.
- 19 R. K. Hocking, E. C. Wasinger, F. M. F. de Groot, K. O. Hodgson, B. Hedman and E. I. Solomon, *J. Am. Chem. Soc.*, 2006, **128**, 10442–10451.
- 20 Y. Nanba and K. Okada, *J. Phys. Soc. Jpn.*, 2010, **79**, 114722.
- 21 Y. Nanba and K. Okada, *J. Electron Spectrosc. Relat. Phenom.*, 2012, **185**, 167–174.
- 22 Y. Nanba, D. Asakura, M. Okubo, Y. Mizuno, T. Kudo, H. S. Zhou, K. Amemiya, J.-H. Guo and K. Okada, *J. Phys. Chem. C*, 2012, **116**, 24896–24901.
- 23 R. D. Cowan, *The Theory of Atomic Structure and Spectra*, University of California Press, Berkeley, CA, 1981.

- 24 F. de Groot and A. Kotani, *Core level spectroscopy of solids*, CRC Press, Boca Raton, FL, 2008.
- 25 M. Matsubara, T. Uozumi, A. Kotani, Y. Harada and S. Shin, *J. Phys. Soc. Jpn.*, 2000, **69**, 1558–1565.
- 26 M. Matsubara, T. Uozumi, A. Kotani, Y. Harada and S. Shin, *J. Phys. Soc. Jpn.*, 2002, **71**, 347–356.
- 27 V. Heine, *Solid State Physics*, Academic Press, New York, 1980, vol. 35, p. 87.
- 28 M. Abbate, F. M. F. de Groot, J. C. Fuggle, A. Fujimori, O. Strebel, F. Lopez, M. Domke, G. Kaindl, G. A. Sawatzky, M. Takano, Y. Takeda, H. Eisaki and S. Uchida, *Phys. Rev. B*, 1992, **46**, 4511–4519.
- 29 J. P. Crocombette, F. J. M. Pollak, N. Thromat and M. Gautier-Soyer, *Phys. Rev. B*, 1995, **52**, 3143–3150.
- 30 J. Fink, T. Müller-Heinzerling, B. Scheerer, W. Speier, F. U. Hillebrecht, J. C. Fuggle, J. Zaanen and G. A. Sawatzky, *Phys. Rev. B*, 1985, **32**, 4899–4904.
- 31 S.-I. Nakai, K. Ogata, M. Ohashi, C. Sugiura, T. Mitsuishi and H. Maezawa, *J. Phys. Soc. Jpn.*, 1985, **54**, 4034–4041.
- 32 S. M. Butorin, *J. Electron Spectrosc. Relat. Phenom.*, 2000, **110-111**, 213–233.
- 33 E. C. Wasinger, F. M. F. de Groot, B. Hedman, K. O. Hodgson and E. I. Solomon, *J. Am. Chem. Soc.*, 2003, **125**, 12894–12906.
- 34 T. Kroll, S. Bonhommeau, T. Kachel, H. A. Dürr, J. Werner, G. Behr, A. Koitzsch, R. Hübel, S. Leger, R. Schönfelder, A. K. Ariffin, R. Mancke, F. M. F. de Groot, J. Fink, H. Eschrig, B. Büchner and M. Knupfer, *Phys. Rev. B*, 2008, **78**, 220502(R).
- 35 W. A. Harrison, *Electronic structure and the properties of solid: the physics of the chemical bond*, Dover Publications, 1989.
- 36 Y. Harada, M. Taguchi, Y. Miyajima, T. Tokushima, Y. Horikawa, A. Chainani, Y. Shiro, Y. Senba, H. Ohashi, H. Fukuyama and S. Shin, *J. Phys. Soc. Jpn.*, 2009, **78**, 044802.